The Version of Record of this article is published in Measurement, and is available online at https://doi.org/10.1016/j.measurement.2026.120565.

HARDWARE DELAY MEASUREMENT FOR BDS TIME TRANSFER RECEIVER WITH SUB-NANOSECOND UNCERTAINTY

Kun Liang[1,*], Yufeng Li[1], Tian Yu[1], Xiangxu Jiao[2], Yuxiang Liu[1], Jian Wang[1]

[1]School of Automation and Intelligence, Beijing Jiaotong University, Beijing 100044, China
[2]Hangzhou Engineering Section of Shanghai Railway Sub bureau, Hangzhou 310011, China
E-mail address: liangk@bjtu.edu.cn

Abstract – Global Navigation Satellite System (GNSS) time transfer is the most popular and widely used way for precise and remote accurate time transfer. With the completion of the BeiDou-3 (BD-3) global constellation, its time transfer precision has been validated; however, calibration remains the primary source for accuracy and uncertainty of time transfer. To resolve the inherent high uncertainty and complexity inherent in existing differential calibration and separately absolute calibration methods, an integrally absolute calibration method was proposed in the paper. The integrally absolute calibration experiments on several GNSS time transfer receivers were conducted and the results of TL07, TL19, GS10 and BJ01 were acquired with the uncertainties of 0.66~0.74 ns for BD-3 B1C signal and 0.66~0.76 ns for BD-3 B2a signal, where were validated effectively through both separately absolute calibration and differential calibration.

***Keywords*: GNSS; BDS; time transfer; timing; absolute calibration**

1. INTRODUCTION

1.1. Overview

At present, we have four GNSS systems, including the Global Positioning System (GPS), GLONASS, the BeiDou Navigation Satellite System (BDS) and Galileo. GPS has been widely used for time transfer for over 40 years since D. W. Allan proposed the method in [1]. It has been playing an essential role in remote clock comparisons for the generation of the International Atomic Time (TAI) [2] and the Coordinated Universal Time (UTC) [3], demonstrating its high precision and reliability in fundamental metrology applications.

With the prompt development of BDS since its completion of BD-3 global signal coverage at the end of 2020, time transfer on the inter-continental and continental links over different baselines have been implemented and validated through comparison with GPS [4-6]. Significant interest has emerged in using BDS for time transfer applications contributing to UTC. The International Bureau of Weights and Measures (BIPM) has been broadcasting predicted UTC information based on BDS and Galileo in its monthly publication Circular T starting in June, 2024.

Hardware delay measurement for GNSS time transfer receiver has been always the most significant premises for the accurate GNSS time transfer. Due to the existence of hardware delay of the receiver, which is relatively fixed and unknown, it is necessary to measure the delay of the time transfer link (calibration of the GNSS time transfer link) for compensation, such as UTC time link calibration. Experience to date has shown that the dominant contribution to the uncertainty of GNSS time transfer is the link calibration [7]. For carrier-phase and code-based time and frequency transfer, the type A uncertainties are 0.3 ns and 0.7 ns, respectively; the type B uncertainty is mainly affected by the hardware delay measurement of the receivers on the time link, i.e. time link calibration. Thus, it can be seen that the combined standard uncertainty of GNSS time and frequency transfer is mainly limited by the receiver hardware delay measurement. Besides, the monitoring of inter-bias among the different GNSS timescales is also based on the accurate compensation of hardware delay for a single GNSS time transfer receiver.

Existing calibration methods include the differential calibration led and studied by the BIPM [8] and the separately absolute calibration, which was first studied and carried out by the National Research Laboratory (NRL) [9]. As of now, separately absolute calibration method generates artificial GNSS signals and observes the difference from the GNSS simulator with the known delay to separately calibrate the three parts: antenna calibration, antenna cable calibration, and receiver host calibration as Figure 1 shows. The complexity of implementation, which involves a series of elaborate measurement steps for each component of a time transfer receiver, could still pose a challenge for further reducing the overall calibration uncertainty. Moreover, for BDS time transfer receiver calibration, however, the discussions are limited to the calibration of the BeiDou-2 (BD-2) link on B1I and B2I. It is necessary to conduct a study on low-uncertainty-level calibrations of BD-3 signals for present applications. If we combine three parts, such as, the receiver host, the antenna and the antenna cable, as a whole component to calibrate, the implied procedures could be acquired to reduce the sources of uncertainty and enhance reliability.

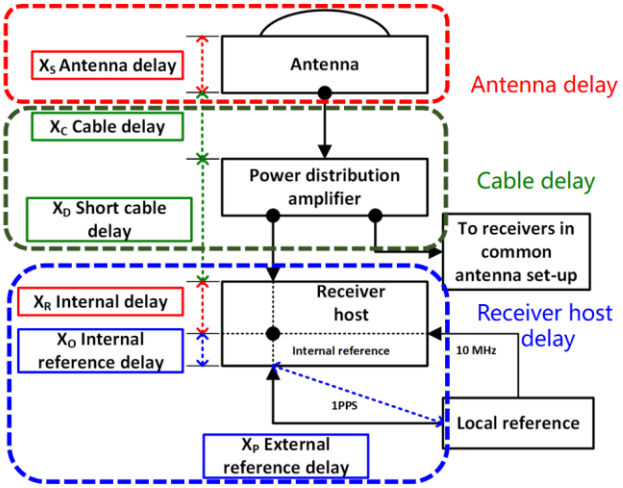

Figure 1. The delays of the receiver

In this paper, we proposes an integrally absolute method, which uses GNSS simulated signals to calibrate the hardware delay of the entire GNSS time transfer receiver. Chapter 3 elaborates on the scheme and theoretical analysis of the integrally absolute calibration method, and verifies the appropriate input power and RF transmission distance for receivers through experiments; Chapter 4 elaborates on the detailed evaluation of uncertainty in the integrally absolute calibration method, including uncertainties introduced by the RF signal, the simulator delay, the RF transmission path, and the receiver reference delay, and presents research on the evaluation of uncertainty in the thermal sensitivity and RF power configuration of receiver; Chapter 5 cross-validates the integrally absolute calibration result and its uncertainty of the receiver hardware delay compared to those of the separately absolute calibration and differential calibration experiments. For each receiver and frequency, the results from the three calibration methods are mutually consistent within their respective uncertainty ranges. The applicability of the method on other GNSS systems is verified with the receiver TL07 in B1I, B3I, B1C, B2a, and L1 C/A. The adaptability of the method on different models, such as, commercial or research-level GNSS time transfer receivers is proofed with the receivers GS10, BJ01, TL07, and TL19 in B1C and B2a.

1.2. Related works

Prior to 2012, the differential calibration method is the primary method involved using a reference receiver maintained by the BIPM (known as the "Golden Receiver") to differentially calibrate receivers at UTC laboratories, achieving a calibration uncertainty at the 5 ns level. Institutions such as the Physikalisch-Technische Bundesanstalt (PTB), the Royal Institute and Observatory of the Navy (ROA), and the National Institute of Metrology (NIM) have conducted improvement research, achieving an optimal uncertainty of 1.5 ns. Since 2012, the BIPM has proposed and initiated the new global calibration campaign, where BIPM only conducting periodic calibrations of GNSS receivers at the designated G1 UTC laboratories by dispatching reference terminal calibrators (also known as traveling receivers) and G1 laboratories implement the calibration for the other UTC laboratories, so-called G2 laboratories [10-11]. Currently, the BIPM conducted and published results based on GPS P1, P2, and C1 codes, as well as Galileo E1 and E5a codes.

Regarding absolute calibration, the concept was first proposed by the U.S. Naval Research Laboratory (NRL), which implemented relevant experiments on an Ashtech Z12-T GPS receiver. In recent years, CNES and the European Space Agency (ESA) have optimized and improved the separately absolute calibration method, specifically regarding transmit antenna delay measurement methods and simulator delay calibration with about 1 ns uncertainty [14-15]. However, in a cross-validation campaign detailed in [16], the consistency of the same receiver calibrated respectively by the ESA and the CNES did not align well within the uncertainty range, showing the deviation can come to 2.67 ns.

The separately absolute calibration involves the separate measurement and calibration of the delays for multiple components, the overall calibration procedure remains relatively cumbersome with numerous sources of uncertainty. In response to this, this paper proposes an integrally absolute calibration method. This approach involves calibrating the total delay of the GNSS receiver components as a unified working unit within a fully anechoic chamber environment. The greatest advantage of the integrally absolute calibration method lies in its simplified measurement steps, eliminating the need for separately absolute calibration of the antenna and antenna cables, thus introducing fewer sources of uncertainty. Consequently, for a single receiver, the combined standard uncertainty of time delay measurement is further optimized to the sub-nanosecond level.

2. METHODS

The principles of the integrally absolute calibration will be thought that the combined hardware delay of the three parts in the time transfer receiver will be calibrated integrally as figure 2 shows. The measurement procedure includes only one main step similar to the receiver host calibration with the antenna and cable together. Subsequently, the uncertainty evaluation will include fewer uncertainty sources from fewer measurement steps.

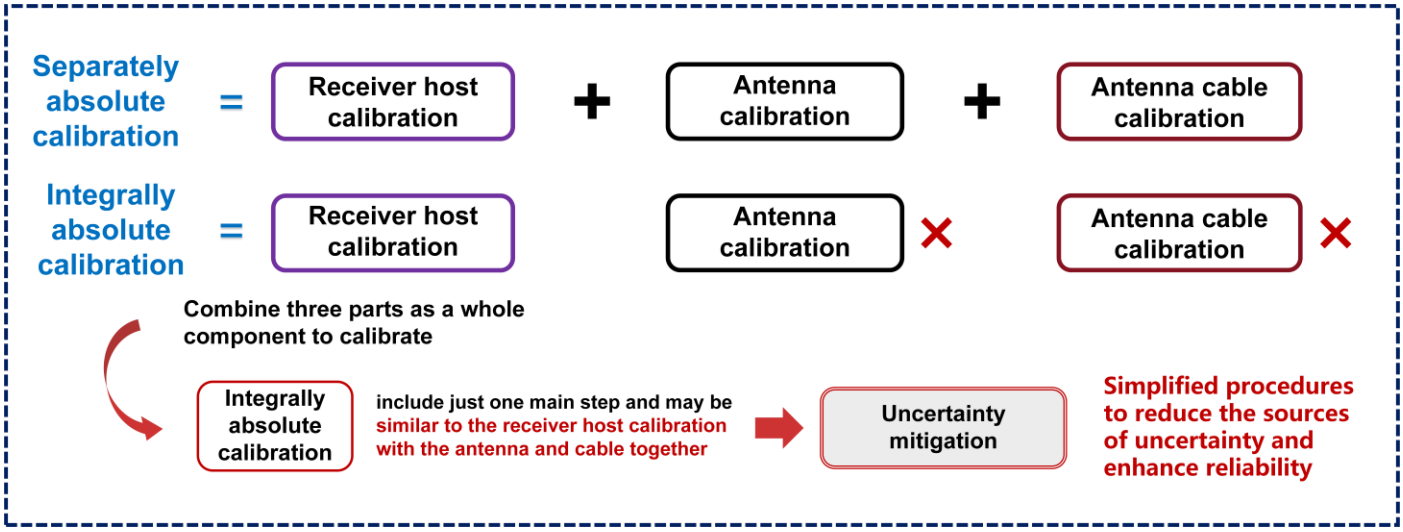

Figure 2. Comparison of the two absolute calibration methods

2.1. Scheme of the calibration

The scheme of the calibration is illustrated in Figure 3. The standard GNSS RF signal is firstly generated in the GNSS simulator, which can be artificially configured and output with high stability and remove any interference. From the transmitting antenna connected to one piece of the antenna cable, the RF signal is broadcast in the air inside an anechoic chamber. The signals arrive at the GNSS time transfer receiver antenna, another piece of antenna cable and the receiver host successively. Finally, the pseudoranges can be solved through the acquisition, tracking, bit synchronization and observation solution and so on. The arrows direct the signal propagation paths. When all the other delays are removed from the overall delay of the RF signal, the hardware delay of the entire receiver could be got. It is noted that the reference time of the GNSS receiver should be unified with the reference of the GNSS simulator. Thus, some measurements for this unification should be given.

In the calibration, the standard GNSS signals are the key element in the measurement scenario. The GNSS constellation simulation is employed for the generation of GNSS signals since the GNSS simulator can artificially emulate the signals with high repeatability and stability, in which the influential factors can be manually eliminated such as the ionospheric and the tropospheric delays. In order to avoid the clutter interference and to reduce multipath effects, the calibration is conducted inside an anechoic chamber. The RF transmission path delay mainly consists of the delay of simulator, the transmitting antenna and the antenna cable, and the distance between the transmitting and receiving antennas. In terms of the OTA measurement rules in the far-field region, the distance between the transmitting and receiving antennas should be maintained in the far-field region to ensure accurate measurement results, as near-field conditions may introduce mutual coupling effects, reactive field interference, and inaccurate characterization of radiation patterns.

The relation for the components' delays in the whole experiment setup can be given in (1) and (2) and the hardware delay of the entire time transfer receiver could be derived as (3).

$$t_{\mathrm{p}} = t_{\mathrm{grx}} + t_{\mathrm{trans}} + t_{\mathrm{sim}} - t_{\mathrm{ref}} \quad (1)$$

$$t_{\mathrm{grx}} = t_{\mathrm{rx}} + t_{cab} + t_{\mathrm{ant}} \quad (2)$$

$$t_{\mathrm{grx}} = t_{\mathrm{p}} - t_{\mathrm{trans}} - t_{\mathrm{sim}} + t_{\mathrm{ref}} \quad (3)$$

t_{p} : overall delay of the RF signal, calculated as the pseudorange difference obtained between the receiver and the simulator;

t_{grx}: hardware delay of the entire time transfer receiver, the sum of the receiver host delay t_{rx}, antenna delay t_{ant} and cable delay t_{cab};

t_{trans}: transmission path delay, the sum of the air gap delay t_{ag}, the transmitting antenna delay t_{horn};

t_{sim}: delays of the simulator and the corresponding cable;

t_{ref}: delay between the receiver clock and the external time reference, the sum of the the external reference $t_{\mathrm{ref-ext}}$ and the internal reference delay $t_{\mathrm{ref-int}}$; in some receivers, this part is automatically measured and compensated for the raw measurements inside the receiver.

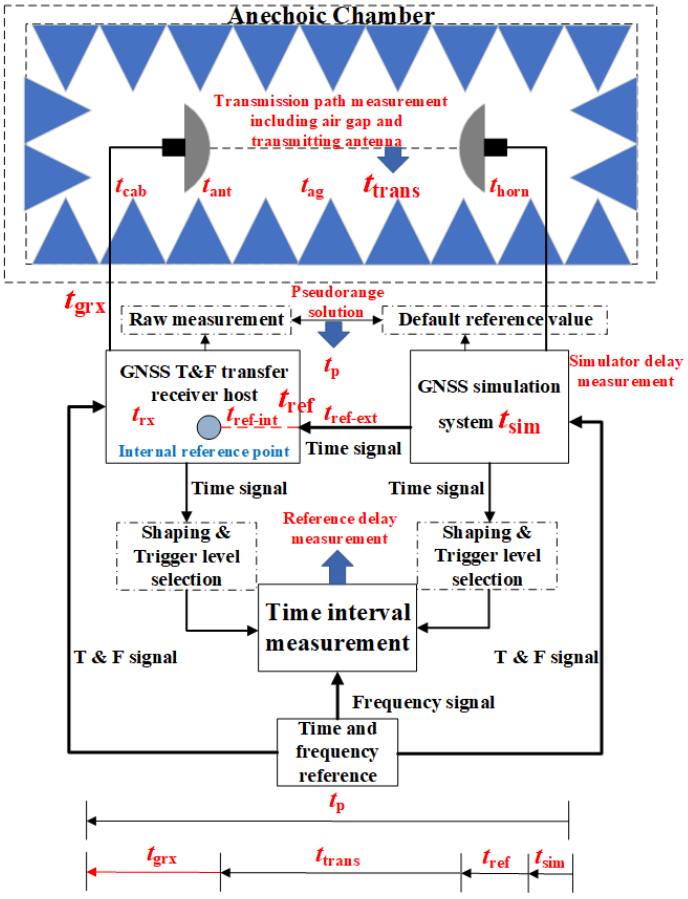

Figure 3. Schematic of the integrally absolute calibration

Detailed procedures uncertainty contribution analysis for the measurement of each component involve the simulator delay, the transmission path delay and the overall signal delay, which will be discussed in the following subsections.

2.2. *Implementation of the calibration*

From the measurement in terms of Figure 4, the overall delay of the RF signal t_p can be derived by deducting the pseudorange data preset in the simulator by the ones observed by the receiver.

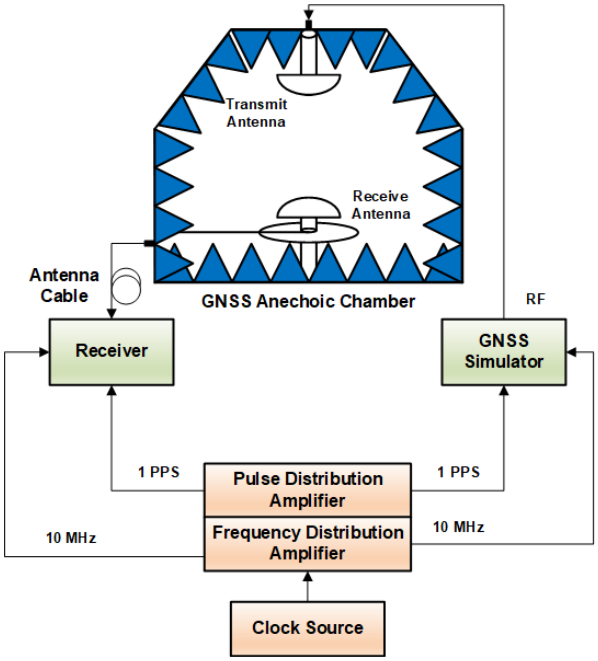

Figure 4. Overall delay measurement of the RF signal

Firstly, the actual GNSS signal arrives at the receiving antenna with a power of about -130 dBm and is amplified by the LNA on the receiver host side to about (-110~-90) dBm. The power level of GNSS signal will significantly affect the signal to noise level for the receiving and moreover measurement noise. Investigation of the different GNSS signal power levels was implemented. Pseudorange measurements in the receiver and reference pseudorange in the simulator were both collected with power level between -110 dBm and -90 dBm, their corresponding time differences were calculated and the statistics were done, such as mean value (mean) and standard deviation (std). -110 dBm for signal arriving at the receiver host side shows best from the statistics in Table 1.

Table 1. Test for pseudorange difference to power level

Power level (dBm)	-110		-100		-90	
Code|Statistics	Mean (ns)	Std (ns)	Mean (ns)	Std (ns)	Mean (ns)	Std (ns)
B1I	116.782	0.078	117.015	0.090	116.287	0.627
L1 C/A	122.034	0.100	122.117	0.152	122.481	0.786

The transmission path delay t_{trans} is defined as the delay experienced by the GNSS signal from the Antenna Phase Centre (APC) of the transmitting antenna to that of the receiving antenna, which thus includes the delay of the air gap t_{ag} and the delay of the transmitting antenna t_{horn} as in (4).

$$t_{\text{trans}} = t_{\text{ag}} + t_{\text{horn}} \tag{4}$$

The former can be measured and calculated by (5), where s stands for the physical distance between the APCs of the two antennas and c stands for the velocity of light in the air.

$$t_{\text{ag}} = \frac{s}{c} \tag{5}$$

The latter is measured as the group delay between the RF connection port of the transmitting antenna and its APC, under an experiment similar to the integrally receiver calibration. Firstly, an observation is completed by directly connecting the cables inside the anechoic chamber as shown in Figure 5 to derive the raw time difference t_0.

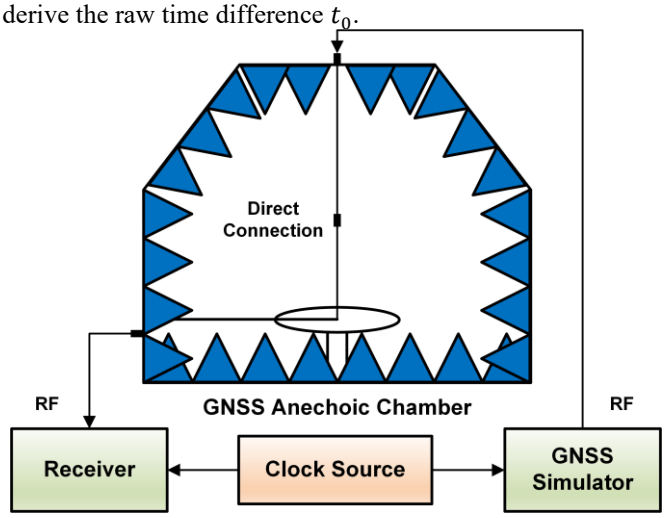

Figure 5. Schematic of the direct connection experiment for transmitting antenna measurement. Some of the instruments are omitted for better viewing

Two identical transmitting antennas will be inserted into the RF signal path then to obtain the according time difference t_{ants} as in Figure 4. Finally, the delay of a single transmitting antenna t_{horn} can be calculated by (6).

$$t_{\text{horn}} = \frac{t_{\text{ants}} - t_0 - t_{\text{ag}}}{2} \tag{6}$$

During the calibration of antennas in the anechoic chamber, antennas under test should be placed in the far field of the transmitting antenna.

$$L > \frac{2D^2}{\gamma} \tag{7}$$

The theoretical value calculated with (7) is 37.4 cm. The appropriate RF transmission distance between transmitting antenna and receiving antenna should be determined since the distance affects the power level of RF signal a lot. When RF power level was set fixed, the tests were conducted by acquiring both pseudorange measurements in the receiver and reference pseudorange in the simulator at some different distances. The corresponding differential time delays between them were calculated. Some std values for the differences are summarized in Table 2.

Table 2. Std for differential time delays at the different distances

Distance (cm)	B1I (ns)	B1C (ns)	B3I (ns)
0	0.26	0.27	0.10
15	0.46	0.40	0.16
60	0.20	0.18	0.07
120	1.02	0.99	0.44
180	0.48	0.45	0.15
300	0.74	0.75	0.28

The measured differential time delays were compared to the theoretical differential time delay values at the different

distances and the difference between them was calculated in Table 3. Combining the results and the practicalities, a distance of 60 cm is selected through a series of experiments. In the experiments, several GNSS time transfer receivers were served to find the most proper RF transmission distance between the transmitting and receiving antennas. All the results with the different receivers can come to the similar conclusion, of which one group results with the receiver TL19 were shown in Table 3.

Table 3. Bias of the measured differential time delays at the different distances

Distance difference (cm)	Theoretical (ns)	B1I (ns)	B1C (ns)	B3I (ns)
15 - 0	0.5	0.81	1.41	-1.70
60 - 0	2	1.45	1.30	-1.86
120 - 0	4	1.48	1.38	-2.42
180 - 0	6	1.25	1.08	-1.68
300 - 0	10	1.40	1.41	-1.82
60 - 15	1.5	0.63	-0.11	-0.16
120 - 15	3.5	0.67	-0.03	-0.72
180 - 15	5.5	0.44	-0.33	0.01
300 - 15	9.5	0.58	0	-0.13
120 - 60	2	0.04	0.07	-0.56
180 - 60	4	-0.19	-0.22	0.18
300 - 60	8	-0.05	0.11	0.03
180 - 120	2	-0.23	-0.30	0.74
300 - 120	6	-0.09	0.03	0.59
300 - 180	4	0.14	0.33	-0.14

After disabling the atmospheric models and excluding all the other settings that might affect, the flip point of the simulated Pseudo Random Noise (PRN) code should be strictly aligned with the time base of the simulator when a specific pseudorange-fixed scenario is broadcast, theoretically. However, due to the coding delay in the digital simulation process of the simulator and the electric delay in its hardware, there will always be a corresponding deviation in practice, that is, the hardware delay of GNSS simulator.

It is calibrated by the three methods, such as, manual reading method, correlation peak method and envelope fitting method. The measurement diagram and manual reading for the simulator delay are shown in Figure 6. The cables intended for connecting to the Pulse Per Second (PPS) and RF input of the receiver are instead connected to the two channels of the oscilloscope respectively for data acquisition as well. By correlation peak method, the acquired RF data will undergo further processing through a coherent demodulation algorithm after down-conversion and low-pass filtering. Meanwhile, the sampled PPS data will be interpolated using a cubic spline to obtain the exact 1V trigger with optimized resolution. A brief description of the algorithm is depicted in Figure 7.

With the same sampling data, in the envelope fitting method the PPS data are processed in the same way as correlation peak method, and the Hilbert transforming is employed to convert the sampling RF data and finally through polyfitting the envelope of RF curves the judgement will be got for the difference between transition point of the RF data and the rising edge of the PPS data. The principle is shown in Figure 8.

For verification, two sets of data were collected for each frequency involving B1I, L1 C/A and B3I, and the measurement results calculated by the three methods in Table 4 were consistent within the range of uncertainty, which effectively validated the accuracy of the simulator hardware delay results with the methods.

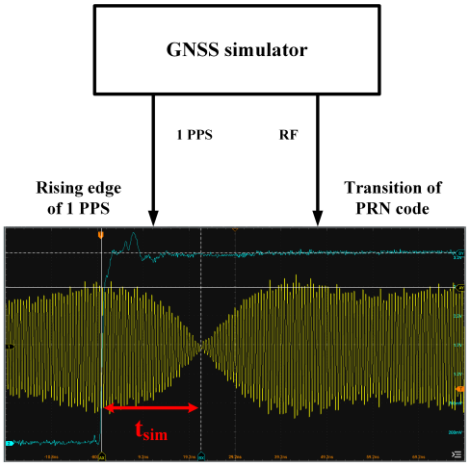

Figure 6. Scheme of the simulator delay measurement

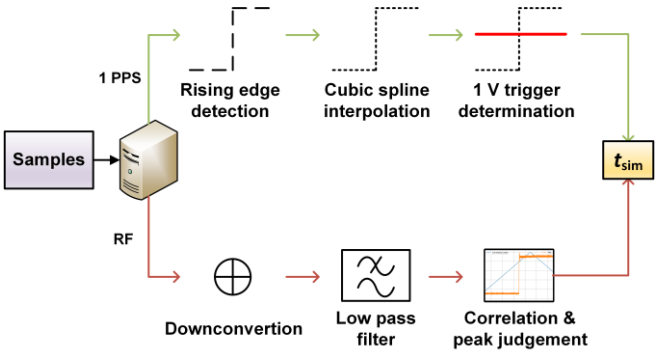

Figure 7. Scheme of the correlation peak method

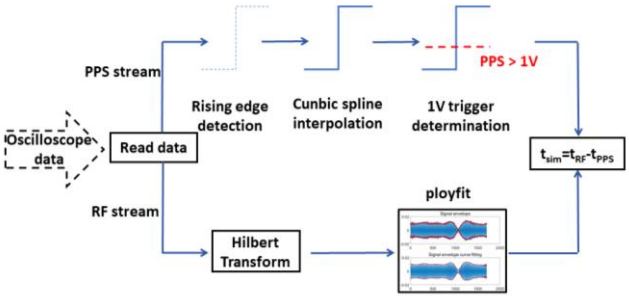

Figure 8. Scheme of the envelope fitting method

Table 4. comparison of the results with three methods for simulator calibration

Codes	Manual reading (ns)	Correlation peak (ns)	Envelope fitting (ns)
BDS B1I	96.8	96.5	96.4
	143.8	143.8	144.1
BDS B3I	91.0	90.9	90.7
	93.6	93.8	92.8
GPS L1 C/A	97.0	96.0	96.3
	143.5	144.4	144.1

After configuring the PPS output of the receiver to synchronize with its internal clock, the reference delay of the receiver can be measured using a time interval counter during the pseudorange observation. The measurements were taken with a rising edge trigger at 1 V for both ports.

The calibration procedures are summarized as Figure 9 shows.

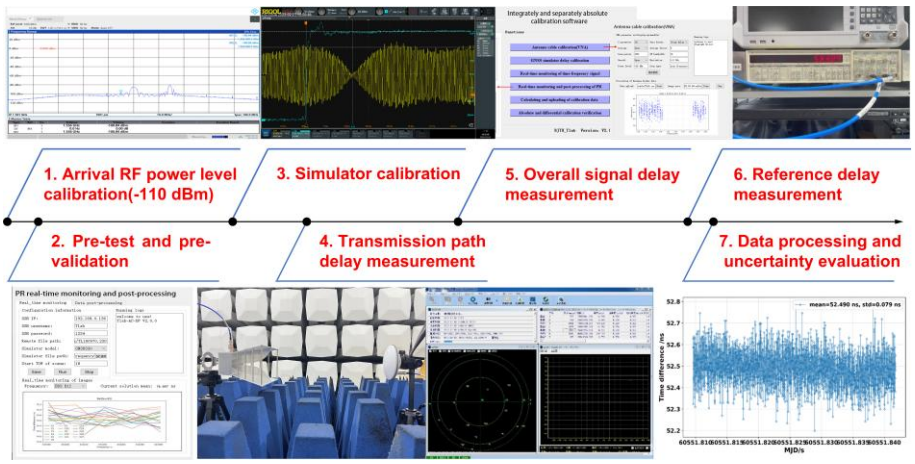

Figure 9. Calibration procedures for integrally absolute calibration

3. UNCERTAINTY EVALUATION

The measurements for the overall delay of the RF signal, the simulator delay, the RF transmission path delay, and the receiver reference delay are involved in the calibration of the receiver. From the calibration scheme and procedures, the sources of uncertainty could be derived from the several delay measurement parts.

In the overall delay measurement of the RF signal, the uncertainty from the inter-channel bias of the simulator u_{bias}, which represents the maximum of the pseudorange delay difference among the time delays solved for the different channels when the simulator broadcasts the same scenario, was taken as 200 ps in combination with the results of multiple measurements. Considering the uncertainty from thermal sensitivity of the receiver u_{temp}, referring to the evaluation procedure on a receiver of the same genre given in [17], we performed a continuous pseudorange difference observation between the receiver and the simulator while manually adjusting the temperatures of the experimental setup. As shown in Figure 10, time difference was calculated from the pseudorange difference divided by speed of light, and the temperature was from the internal measurement of the receiver. Since the obvious linear characteristics of both time difference and temperature and their correlation, a temperature coefficient of 0.024 ns/℃ was derived by linear fitting. Due to the variations in ambient temperature during calibration are often logged within a range of ±2 ℃, the uncertainty of the term was conservatively taken as 192 ps, based on a rectangular distribution. The uncertainty from the switching feature of the receiver $u_{\text{switch-rx}}$, which represents the maximum bias in recording the pseudorange delay difference before and after restarting the receiver under the same experiment condition, was taken as 173 ps based on a rectangular distribution.

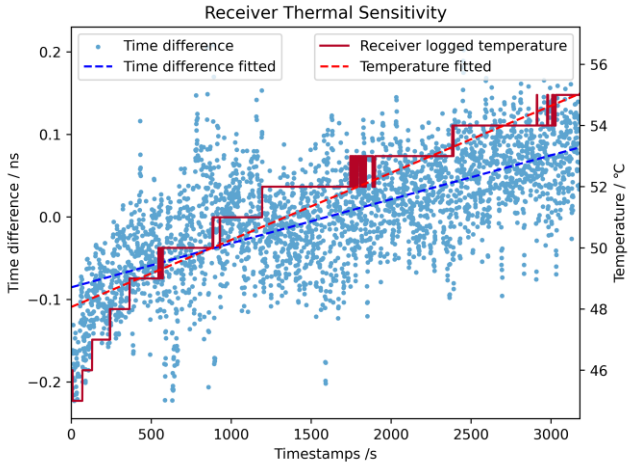

Figure 10. Overall system delay variations (with respect to the mean) caused by different environmental temperatures

The uncertainty u_{power} is sourced from the Radio Frequency (RF) power configuration. Referring to the evaluation in [14] when the Automatic Gain Control (AGC) is maintained at the linear area, we did the sampling with altering the output level of the simulator as shown in Figure 11. The corresponding AGC of the receiver was logged, and a power coefficient of 0.012 ns/dB was ultimately derived. Due to the variations in AGC during calibration are logged within a range of ±1 dB, the uncertainty of the term was conservatively taken as 100 ps. The uncertainty u_{rep} introduced by the repeatability of measurements, is taken as the maximum standard deviation of the solved pseudorange delay difference.

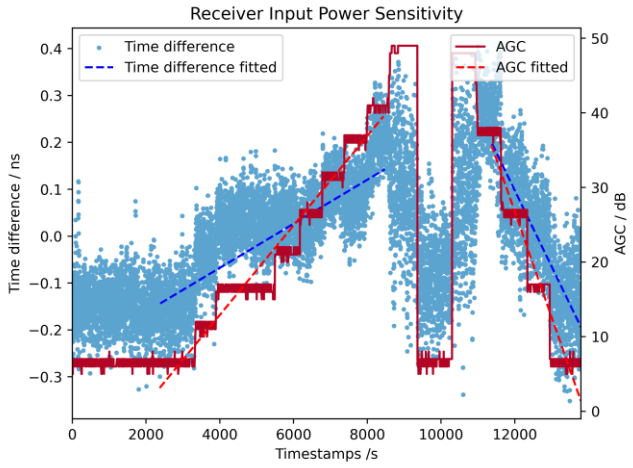

Figure 11. Overall delay variations (with respect to the mean) caused by different input powers, characterized by AGC of the receiver

The uncertainty in the overall delay measurement can thus be derived by (8).

$$u_{\mathrm{OD}} = \sqrt{u_{\mathrm{bias}}^2 + u_{\mathrm{temp}}^2 + u_{\mathrm{switch-rx}}^2 + u_{\mathrm{power}}^2 + u_{\mathrm{rep}}^2} \quad (8)$$

In the measurement of transmission path delay, APC stability leads to the uncertainty u_{APC}, and its conservative value can be extrapolated from the typical value of APC stability given in the calibration example of the Chinese National Metrology Technical Specification JJF 1403-2013 [18], taken as 5 ps. The other sources of uncertainty in this procedure also include:

$u_{\mathrm{switch-rx}}, u_{\mathrm{power}}, u_{\mathrm{bias}}, u_{\mathrm{temp}}$, the switching feature of the receiver, is evaluated in the same way as the uncertainty evaluation does in the overall delay measurement.

The uncertainty of the transmission path delay measurement can thus be derived by (9).

$$u_{\mathrm{TPD}} = \sqrt{u_{\mathrm{APC}}^2 + u_{\mathrm{switch-rx}}^2 + u_{\mathrm{power}}^2 + u_{\mathrm{bias}}^2 + u_{\mathrm{temp}}^2} \quad (9)$$

In the simulator delay measurement, the uncertainty from the resolution of the oscilloscope, is taken as 100 ps under a default sampling rate of 10 GSa/s.u_{trig}, the uncertainty from the trigger error of the oscilloscope, is taken as 200 ps according to the instrument's manual. The uncertainty u_{rep} introduced by the repeatability of measurements, is taken as the maximum standard deviation of the solved simulator delay and conservatively extended to 300 ps.

The uncertainty $u_{\mathrm{switch-sim}}$ from the switching feature of the simulator was evaluated using the maximum bias in the simulator delay solutions before and after restarting the simulator while the simulator always broadcasts the same scenario for 10 restarts. In this evaluation, the PPS and RF measurement per second was collected 10 minutes after the simulator signal was observed steadily, each set of data contains one cycle of PRN code sampling points for the required frequency, and then the offline data is processed using the correlation peak method to obtain a maximum bias of 500 ps. Based on a rectangular distribution, the $u_{\mathrm{switch-sim}}$ is taken as 289 ps.

Similarly,u_{power}introduced by the RF power configuration, is evaluated the same way, taken as 115 ps.

The uncertainty of the simulator delay measurement can thus be derived by (10).

$$u_{\mathrm{SD}} = \sqrt{u_{\mathrm{res}}^2 + u_{\mathrm{trig}}^2 + u_{\mathrm{rep}}^2 + u_{\mathrm{switch-sim}}^2 + u_{\mathrm{power}}^2} \quad (10)$$

Finally, the combined standard uncertainty is evaluated from the above parts. Compared with the separately absolute calibration, the uncertainty sources from antenna calibration and antenna cable calibration were removed.

4. EXPERIMENTS AND VERIFICATION

The experiments are setup and implemented for the validation of the integrally absolute calibration.

4.1. Validation method

Separately absolute calibration and differential calibration methods were performed to validate the results. The main differences between the separately absolute calibration method and the proposed method lie in the separately absolute calibration of the receiver host delay t_{host} by directly connecting the cables inside the anechoic chamber and thus removing the measurement of t_{trans}, and instead appending the measurement of the receiver antenna delay t_{ant} through a procedure similar to that described in 2.1, and the individual calibration of the antenna cable delay t_{cab} using a Vector Network Analyzer (VNA). The measurements of the simulator delay and the reference delay stay the same as the integrally absolute calibration. The hardware delay of the entire time transfer receiver in the separately absolute calibration can thus be given in (11).

$$t_{\mathrm{grx}} = t_{\mathrm{rx}} + t_{\mathrm{ant}} + t_{\mathrm{cab}} = t_{\mathrm{p}} - t_{\mathrm{sim}} + t_{\mathrm{ref}} + t_{\mathrm{ant}} + t_{\mathrm{cab}} \quad (11)$$

The sources of uncertainty in the receiver antenna calibration procedure include u_{APC}, $u_{\mathrm{switch-rx}}$, u_{bias} and u_{temp} as similarly evaluated in 2.3, with the addition of the u_{rep} introduced by the repeatability of measurements and the existing uncertainty of transmission path delay measurement t_{trans}. The uncertainty of the transmission path delay measurement can thus be derived by (12).

$$u_{\mathrm{RAD}} = \sqrt{\begin{matrix} u_{\mathrm{APC}}^2 + u_{\mathrm{switch-rx}}^2 + u_{\mathrm{power}}^2 \\ +u_{\mathrm{bias}}^2 + u_{\mathrm{temp}}^2 + u_{\mathrm{rep}}^2 + u_{\mathrm{trans}}^2 \end{matrix}}. \quad (12)$$

The sources of uncertainty in the antenna cable calibration procedure include:

u_{cal} : uncertainty introduced by the initial two-port calibration of the VNA, taken as 200 ps referring to a similar evaluation in [15];

u_{deform}: uncertainty introduced by the cable deformation, taken as 150 ps referring to [17];

u_{temp}: the thermal sensitivity of the antenna cable, taken as 23 ps based on a rectangular distribution, derived by a temperature coefficient of 0.024 ns/°C referring to [17] with the ±2 °C range of logged ambient temperature during the calibration;

u_{cnctr} : uncertainty introduced by the utilization of connectors, taken as 400 ps;

u_{rep} : uncertainty introduced by the repeatability of measurements, taken as the standard deviation of the samples.

The uncertainty of the antenna cable delay measurement can thus be derived by (13).

$$u_{\mathrm{ACD}} = \sqrt{u_{\mathrm{cal}}^2 + u_{\mathrm{deform}}^2 + u_{\mathrm{temp}}^2 + u_{\mathrm{cnctr}}^2 + u_{\mathrm{rep}}^2}\,. \tag{13}$$

By now, the total uncertainty of the separately absolute calibration can be expressed in (14).

$$U = \sqrt{u_{\mathrm{OD}}^2 + u_{\mathrm{RAD}}^2 + u_{\mathrm{SD}}^2 + u_{\mathrm{RD}}^2 + u_{\mathrm{ACD}}^2}\,. \tag{14}$$

Figure 12 shows the basic principles of differential calibration. For the Common Clock Difference (CCD) experiment, the GNSS receiver to be calibrated and the reference GNSS receiver with known delay are connected to the same clock. The same-period observation is then performed under the condition of ultra-short baseline. The differential observation data Δt_{CCD} can be obtained through differential processing of the total delay between the equipment to be calibrated (DUT) and the reference equipment (REF). This processing method can eliminate most irrelevant errors from the ionosphere, troposphere, and multipath effects simultaneously due to the arrangement of the stations according to the ultra-short baseline.

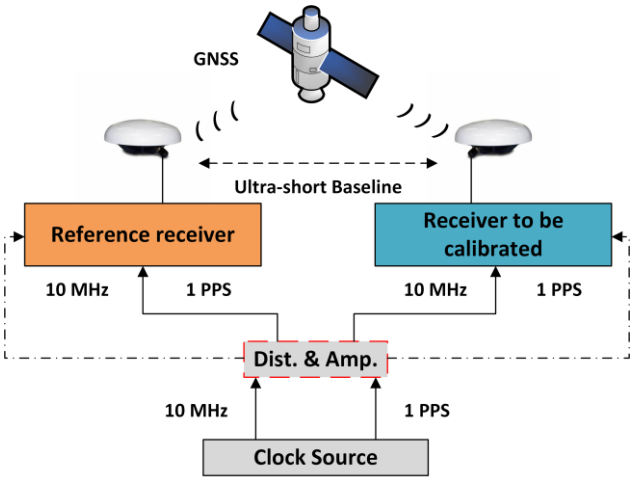

Figure 12. Principle of the differential calibration

Finally, the differential calibration value for each frequency code can be calculated using (15). INT DLY, REF DLY, and CAB DLY represent hardware delay for the receiver host and the antenna, reference delay, and antenna cable delay, respectively. The uncertainty evaluation is detailed in [7] and [8].

$$\begin{aligned} \mathrm{INT\ DLY_{DUT}} + \ & \mathrm{CAB\ DLY_{DUT}} \\ & = \Delta t_{\mathrm{CCD}} \\ & + (\mathrm{REF\ DLY_{DUT}} - \mathrm{REF\ DLY_{REF}} \\ & + \mathrm{CAB\ DLY_{REF}} + \mathrm{INT\ DLY_{REF}}) \end{aligned} \tag{15}$$

4.2. Calibration system

We have built the calibration system as shown in Figure 13 based on the requirements through the aforementioned theoretical analysis, which includes clock sources, a self-designed anechoic chamber shown in Figure 14 and modules for GNSS simulation, time frequency distribution, precise measurement, data processing and calibration solution.

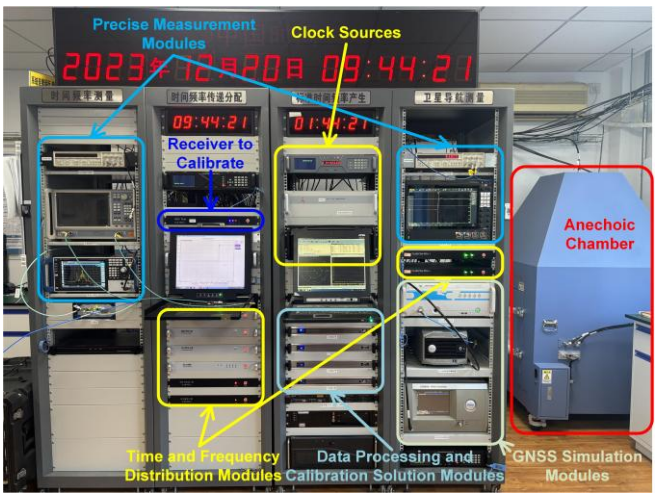

Figure 13. Schematic of the calibration system

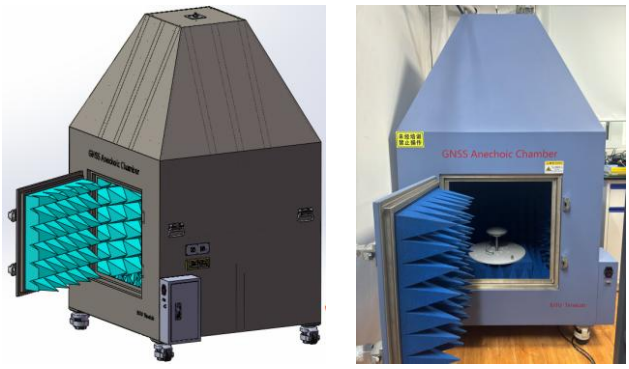

Figure 14. Blueprint and actual shot of the self-designed anechoic chamber, equipped with a controllable one-dimensional rotatable platform

The GNSS simulator utilized in the experiment was a MATRIX GNS8330, which is able to generate BDS B1C and B2a signals in the same scenario, and emulate the full constellations including GEO, IGSO and MEO satellites for BDS system. Before we employ the simulator in the measurement, its performances, such as stability and noise level, have been verified and exhibited with the differences between the reference pseudoranges in the simulator and the ones measured via the receiver. A self-developed absolute calibration software for post-processing in Figure 15 and monitoring of pseudorange measurement monitoring in real time was developed deployed as figure shows. Figures 16 and 17 separately in BDS B1C and B2a codes show the typical examples for the performances.

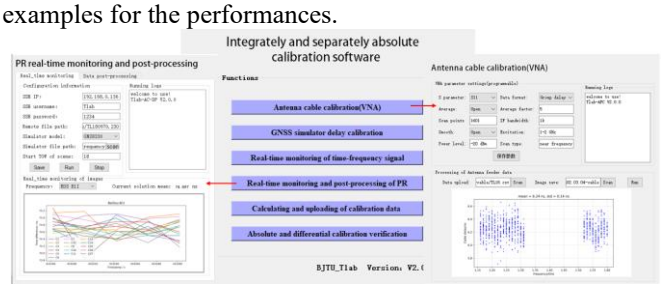

Figure 15. Absolute calibration processing software

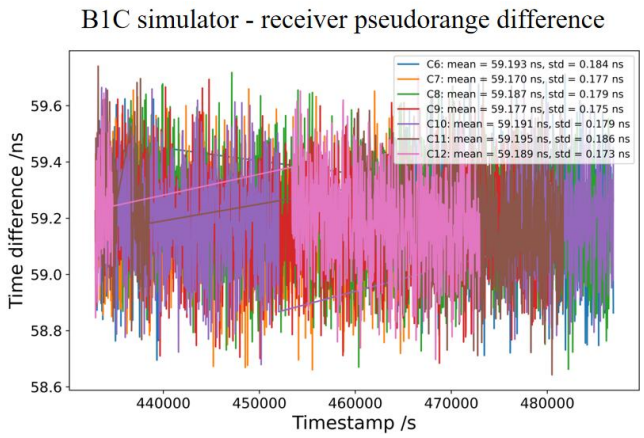

Figure 16. Pseudorange performance of the simulated B1C signals

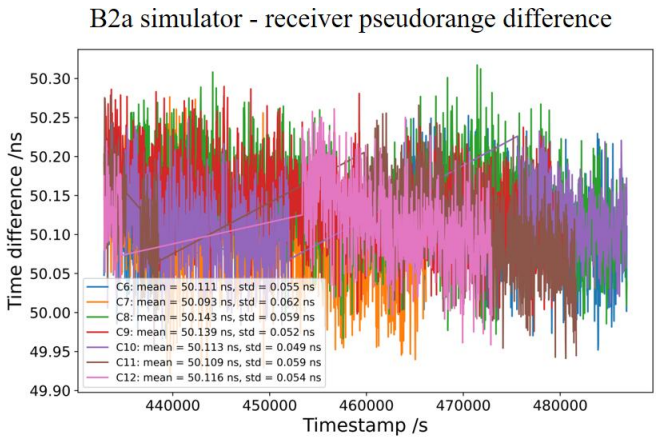

Figure 17. Pseudorange performance of the simulated B2a signals

The calibration experiments were carried out on a homemade TLab-TFS-G1 type GNSS time transfer receiver, coded TL19, as shown in Figure 18. It is capable of acquiring multiple GNSS signals to generate the Receiver Independent Exchange Format (RINEX) and the Common GNSS Generic Time Transfer Standard (CGGTTS) files, thus to achieve remote comparisons through the GNSS All in View (AV), Common View (CV) and the Carrier Phase (CP).

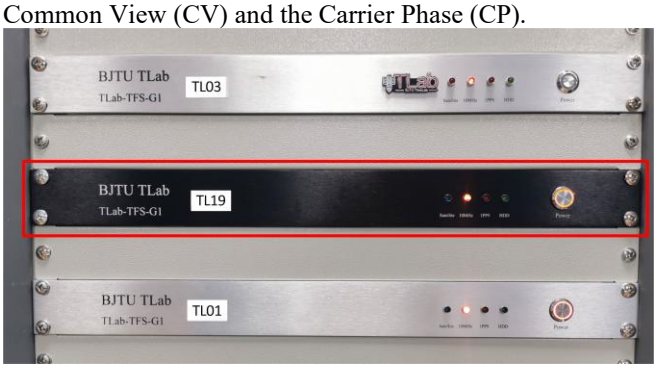

Figure 28. Homemade GNSS time transfer receiver TLab-TFS-G1

4.3. Results and uncertainty

The overall delay was solved during a 10,000-second observation with a sample interval of 30 s, as shown in Figure 19 and Figure 20. The final result t_p will be the average of all satellite solutions for the same signal, that is, 320.963 ns for B1C and 315.977 ns for B2a.

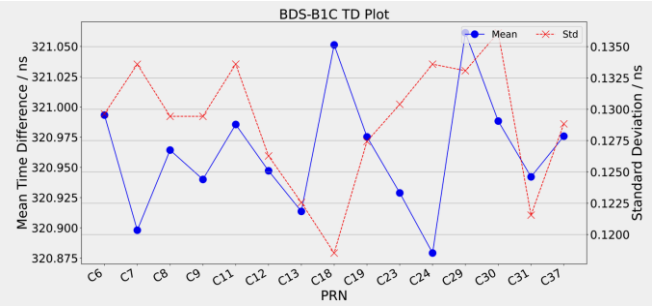

Figure 19. Results of the overall delay for B1C

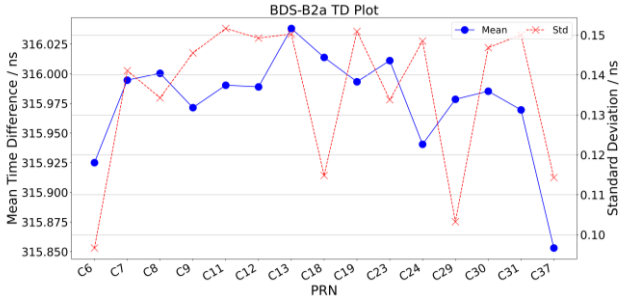

Figure 20. Results of the overall delay for B2a

In terms of (8), we evaluated the uncertainty of this procedure at 407 ps and 443 ps for B1C and B2a signals, respectively, as shown in Table 5. The type A uncertainty was evaluated by the statistical analysis of a series of observations and the type B by means other than the statistical analysis of a series of observations, according to the Guide to the Expression of Uncertainty in Measurement (GUM).

Table 5. Uncertainty budget for the overall system delay measurement

Contribution	Type	Standard uncertainty for B1C (ps)	Standard uncertainty for B2a (ps)
u_{bias}	B	200	200
u_{temp}	B	192	192
$u_{\text{switch-rx}}$	B	173	173
u_{power}	B	100	100
u_{rep}	A	220	282
$\boldsymbol{u_{\text{OSD}}}$		**407**	**443**

Following the procedures outlined in section 2.2, we used here a pair of identical horn antennas to obtain the transmission path delay of 3.148 ns for B1C and 3.003 ns for B2a.

The uncertainty of this procedure was evaluated at 342 ps according to (9), calculated as the combined square root sum of the contributing factors listed in Table 6.

Table 6. Uncertainty budget for the transmission path delay measurement

Contribution	Type	Standard uncertainty (ps)
u_{APC}	B	5
$u_{\text{switch-rx}}$	B	173
u_{power}	B	100
u_{bias}	B	200
u_{temp}	B	192

u_{OSD}	**342**

According to section 2.2, a specific scenario with zero pseudorange was broadcast using only one satellite. The samples were taken by a multi-channel oscilloscope and then sent to the post processing software.

Taking B1C as an example, after interpolation and the correlation processing, the simulator calibration yielded 97.100 ns for B1C and 84.700 ns for B2a, as shown in Figure 21. The uncertainty of this procedure in terms of (10) was evaluated at 486 ps, as shown in Table 7.

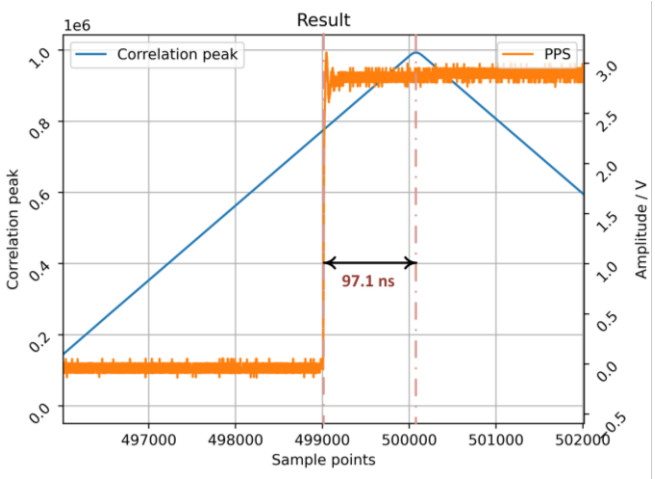

Figure 21. Results of the simulator delay calibration for B1C (left) and B2a (right)

Table 7. Uncertainty budget for the simulator delay measurement

Contribution	Type	Standard uncertainty (ps)
u_{res}	B	100
u_{trig}	B	200
u_{rep}	A	300
$u_{switch-sim}$	B	289
u_{power}	B	115
u_{OD}		**486**

The reference delay was acquired from the counter measurements during the pseudorange observation after delay compensations for pivot cables, and yielded 29.925 ns as shown in Figure 22.

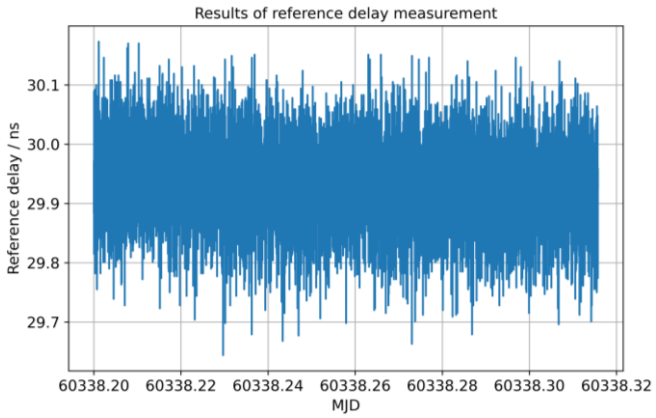

Figure 22. Results of the reference delay measurement

The uncertainty of this procedure was evaluated at 136 ps, as shown in Table 8.

Table 8. Uncertainty budget for the reference delay measurement

Contribution	Type	Standard uncertainty (ps)
u_{res}	B	100
u_{trig}	B	50
u_{rep}	A	77
u_{RD}		**136**

The total standard uncertainty for calibration was the combination of the above several uncertainty contribution items, which is 0.74 ns for B1C and 0.76 ns for B2a, respectively. By now, the integrally absolute calibration results and the corresponding uncertainties for TL19 receiver can be derived and are listed in Table 9.

Table 9. Integrally absolute calibration results for BD-3 signals (ns)

	t_p	t_{trans}	t_{sim}	t_{ref}	t_{grx}	U
B1C	320.963	3.148	97.100	29.925	250.64	0.74
B2a	315.977	3.003	84.700	29.925	258.20	0.76

4.4. Results validation with other calibration

The separately absolute calibration was performed sharing the nearly same calibration system due to the similar instrumental requirements. The experimental setup for the overall delay measurement stays the same as in 3.2 and obtained the result t_p of 75.774 ns for B1C and 72.142 ns for B2a, as shown in Figure 23 and Figure 24.

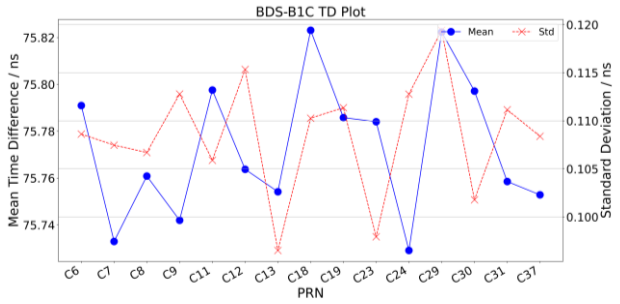

Figure 23. Results of the overall system delay for B1C

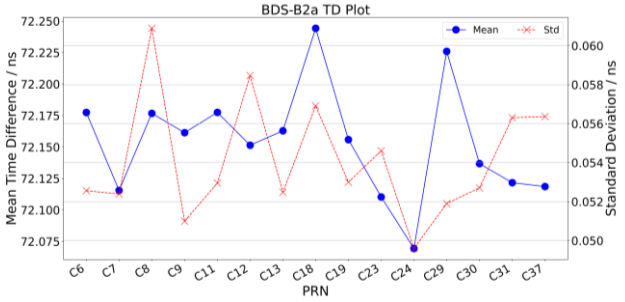

Figure 24. Results of the overall system delay for B2a

Combining the five effects similar to (8), we evaluated the uncertainty of this procedure at 362 ps and 349 ps for B1C and B2a signals, respectively.

Following the procedures outlined in 2.3, we used here a pair of identical horn antennas to obtain the receiver antenna

delay of 15.883 ns for B1C and 16.907 ns for B2a. The uncertainty of this procedure was evaluated at 506 ps and 515 ps, calculated as the combined square root sum of the contributing factors listed in (12).

The measurements of the antenna cable delay were obtained using a VNA in the frequency band of (1.16~1.31) GHz and (1.51~1.62) GHz, which are able to cover all present GNSS carrier frequencies, as shown in Figure 25.

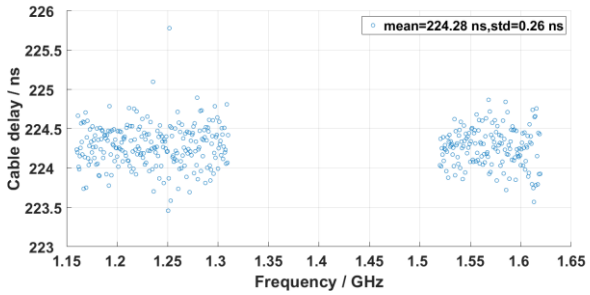

Figure 35. Results of the antenna cable delay measurement

The measurement result is 224.28 ns and the uncertainty of this procedure was evaluated at 539 ps, calculated as the combined square root sum of the contributing factors listed in Table 10.

Table 10. Uncertainty budget for the receiver antenna delay measurement.

Contribution	Type	Standard uncertainty (ps)
u_{cal}	B	200
u_{deform}	B	150
u_{temp}	B	23
u_{cnctr}	B	400
u_{rep}	A	260
$\boldsymbol{u_{\mathrm{ACD}}}$		**539**

The simulator delay yielded 96.500 ns for B1C and 83.480 ns for B2a as the same procedure in 3.4 with the uncertainty of 486 ps. The reference delay was measured as 29.983 ns with the uncertainty of 136 ps.

Adding the additional antenna delay and antenna cable delay measurements brings the combined standard uncertainty of the separately absolute calibration to 0.97 ns for both B1C and B2a in accordance with (14). The calibration results for TL19 receiver can be derived in Table 11.

Table 11. Separately absolute calibration results for BD-3 signals (ns)

	t_{p}	t_{sim}	t_{ref}	t_{ant}	t_{cab}	t_{grx}	U
B1C	75.774	96.500	29.983	15.883	224.28	249.42	0.97
B2a	72.142	83.480	29.983	16.907	224.28	259.83	0.97

The differential calibration was conducted with the aid of a calibrated BDS time transfer receiver, code BJ01 under an ultra-short baseline setup for co-observation with the TL19, as shown in Figure 26.

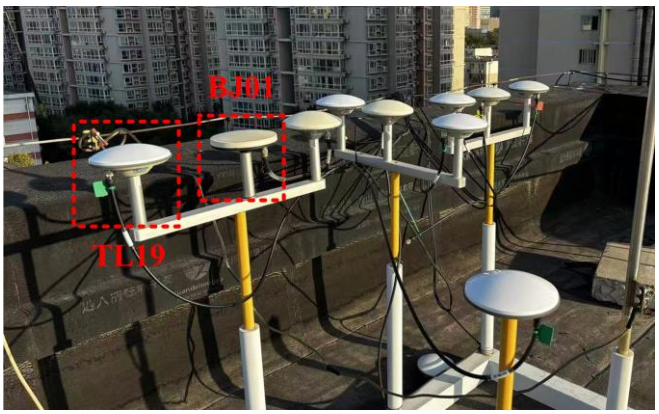

Figure 46. Ultra-shortbaseline setup for differential calibration of TL19

The absolute-calibrated delay parameters of BJ01 are listed in Table 12.

Table 12. Delay parameters of BJ01 and TL19 (ns)

		INT DLY	CAB DLY	REF DLY
BJ01	B1C	27.12	210.18	0.00
	B2a	29.55	210.18	0.00
TL19	B1C	/	224.28	53.42
	B2a	/	224.28	53.42

The CCD results Δt_{CCD} in B1C and B2a are respectively -39.52 ns and -35.27 ns, as shown in Figure 27 and 28.

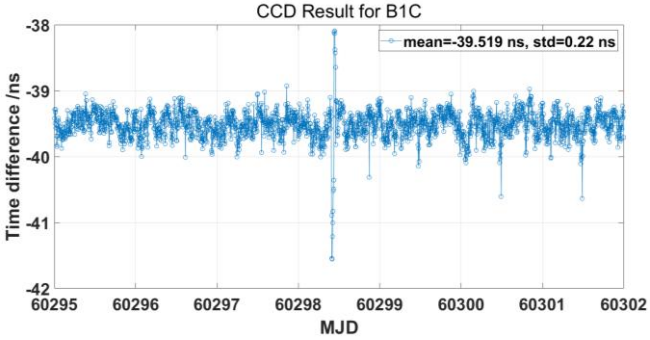

Figure 57. CCD result for B1C in differential calibration

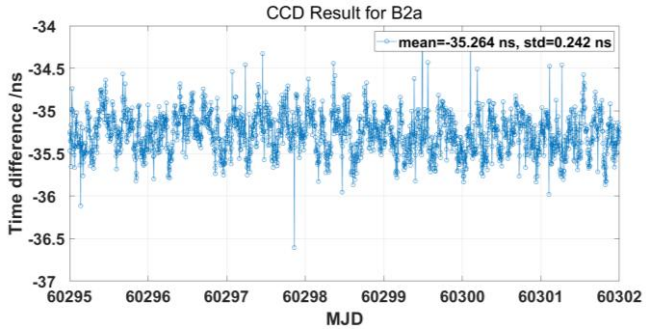

Figure 68. CCD result for B2a in differential calibration

The receiver calibration results for B1C and B2a are 251.20 ns and 257.88 ns respectively, and the uncertainties were evaluated at 1.32 ns and 1.33 ns, calculated as the combined square root sum of the contributing factors listed in Table 13.

Table 13. Uncertainty budget for the differential calibration.

Contribution	Type	Standard uncertainty	Standard uncertainty

		for B1C (ps)	for B2a (ps)
u_{rep}	A	220	242
u_{proc}	B	430	430
u_{ref}	B	707	707
$u_{\mathrm{ref-cal}}$	B	660	660
u_{cab}	B	763	763
$\boldsymbol{u_{\mathrm{ACD}}}$		**1323**	**1327**

The calibration results using three different methods aligned within the uncertainty range, as shown in Figure 29, confirming the validity of the proposed method.

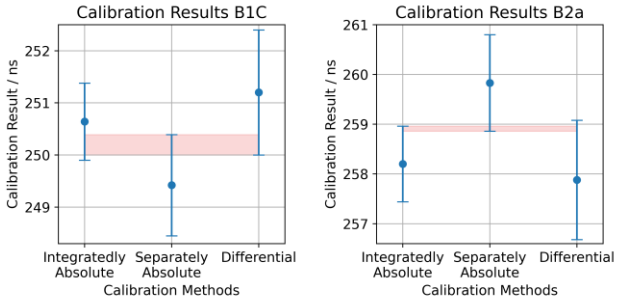

Figure 29. Results of the three calibration methods

4.5. Applicability for different GNSS systems and different types of receivers

The proposed integrally absolute calibration method is equally applicable to other GNSS systems. To further validate this, we conducted the calibration experiments using an another homemade GNSS time transfer receiver (TLab-TFS-G1, coded TL07). TL07 was calibrated for codes including BDS B1I, B3I, B1C, and B2a; GPS L1 C/A; and Galileo E1. The integrally absolute calibration results, along with the separately absolute calibration results and their corresponding uncertainties for the TL07 receiver are summarized in Table 14.

Table 14. Absolute calibration results for TL07 (ns)

Type	Signal	t_{grx}	U
Integrally absolute calibration	B1I	251.19	0.69
	B3I	251.98	0.67
	B1C	252.57	0.68
	B2a	254.42	0.66
	L1 C/A	251.52	0.68
	E1	245.86	0.67
Separately absolute calibration	B1I	250.94	0.96
	B3I	251.78	0.93
	B1C	252.70	0.94
	B2a	254.95	0.92
	L1 C/A	252.79	0.95
	E1	247.41	0.92

Simultaneously, the absolute calibration experiments were conducted for the BDS B1C and B2a codes on several GNSS time transfer receivers. The different types of receivers were involved, such as the TMS10 type GNSS time transfer receiver GS10, the TF-GNSS-200B type GNSS time transfer receiver BJ01, the homemade TLab-TFS-G1 type GNSS time transfer receiver TL07 and TL19. The calibration results for each receiver are summarized in Table 15. The agreement between the separately calibration and integrally calibration was acquired from the results of all receivers used in the experiments and achieves a sub-nanosecond level of uncertainty with integrally calibration.

Table 15. Absolute calibration results for different types of receivers (ns)

Type	Receiver	Signal	t_{grx}	U
Integrally absolute calibration	GS10	B1C	207.33	0.67
		B2a	208.01	0.68
	BJ01	B1C	237.30	0.66
		B2a	239.73	0.66
	TL07	B1C	252.57	0.68
		B2a	254.42	0.66
	TL19	B1C	250.64	0.74
		B2a	258.20	0.76
Separately absolute calibration	GS10	B1C	206.83	0.92
		B2a	207.88	0.93
	BJ01	B1C	237.00	0.91
		B2a	240.03	0.91
	TL07	B1C	252.70	0.94
		B2a	254.95	0.92
	TL19	B1C	249.42	0.97
		B2a	259.83	0.97

5. CONCLUSIONS

We developed an integrally absolute calibration method dedicated to BDS time transfer receivers towards future applications. The calibration considers the entire time transfer receiver as a whole unit to measure its hardware delay, instead of performing a series of elaborate procedures designed for each component of the receiver.

We built an absolute calibration system including various measurement modules to satisfy the requirements of the calibration experiments. The calibration uncertainty budget was thus optimized to well below 1 ns due to the removal of some measurement procedures such as the receiver antenna calibration and the cable calibration.

To verify the proposed calibration method, as well for the applicability for different GNSS systems and different types of receivers, we conducted the measurements with several GNSS time transfer receivers, compared to separately absolute calibration or differential calibration. The combined standard uncertainties for integrally absolute calibration, separately absolute calibration and differential calibration were 0.66~0.76 ns, 0.91~0.97 ns and about 1.3 ns respectively. Alignments in the uncertainty range were reached across the three different methods, which showed favourable consistency.

ACKNOWLEDGMENTS

This work was supported by the Yantai Major Science & Technology Innovation and Development Project (2024ZDCX002) and the TaiShan Industrial Experts Program (tscx202408155), the National Natural Science Foundation of China with Grant No. 12473072, the Open Foundation of The Center of National Railway Intelligent Transportation System Engineering and Technology (2023YJ360).

REFERENCES

[1] D. W. Allan, M. A. Weiss, **Accurate time and frequency transfer during common-view of a GPS satellite**, Proceedings of the 34th Annual Symposium on Frequency Control (IEEE), 1980, pp. 334-346.

[2] G. Petit, F. Arias, G. Panfilo, **International atomic time: Status and future challenges**, Comptes Rendus Physique, 2015, 16(5), pp. 480-488.

[3] G. Panfilo, F. Arias, **The coordinated universal time (UTC)**, Metrologia, 2019, 56(4), 042001.

[4] W. Guang, J. Zhang, H. Yuan, W. Wu, S. Dong, **Analysis on the time transfer performance of BDS-3 signals**. Metrologia, 2020, 57(6), 065023.

[5] Z. Ren, H. Gong, D. Lyu, J. Peng, Y. Guo, **Time transfer with BDS-3 signals: CV, PPP and IPPP**. Measurement Science and Technology, 2023, 34(4), 045007.

[6] Y. Ge, X. Cao, D. Lyu, Z. He, F. Ye, **An investigation of PPP time transfer via BDS-3 PPP-B2b service**. GPS Solutions, 2023, 27(2), 61.

[7] Z. Jiang, **Total Delay and Total Uncertainty in UTC Time Link Calibration-A BIPM Pilot Study**, Proceedings of the 45th Annual Precise Time and Time Interval Systems and Applications Meeting, 2013, pp. 112-125.

[8] G. Petit, P. Defraigne, B. Warrington, P. Uhrich, **Calibration of dual frequency GPS receivers for TAI**, Proceedings of the 20th European Frequency and Time Forum (IEEE), 2006, pp. 455–9.

[9] J. White, R. Beard, G. Landis, G. Petit, E. Powers, **Dual frequency absolute calibration of a geodetic GPS receiver for time transfer**, Proceedings of the 15th European Frequency and Time Forum, 2001, pp. 167–72.

[10] Z. Jiang , G. Petit, F. Arias, **BIPM calibration scheme for UTC time links—BIPM pilot expermiment to strenghen Asia-Europe very long baselines**, 2011 Joint Conference of the IEEE International Frequency Control and the European Frequency and Time Forum (FCS) Proceedings, IEEE, 2011, 1-6.

[11] G. Petit, P. Defraigne, **Calibration of GNSS stations for UTC**, Metrologia, 2023, 60(2), 025009.

[12] M. Lombardi, **A NIST disciplined oscillator: Delivering UTC (NIST) to the calibration laboratory**, NCSLi Measure, 2010, 5(4), 46-54.

[13] K. Liang, Q. Chen, K. Han, Z. Yang, A. Zhang, **Replicating UTC (NIM) remotely for time and frequency traceability**, International Journal of Electrical Engineering, 2019, 26(4), 147-155..

[14] D. Valat, J. Delporte, **Absolute calibration of timing receiver chains at the nanosecond uncertainty level for GNSS time scales monitoring**, Metrologia, 2020, 57(2), 025019 (14pp).

[15] E. Garbin, P. Defraigne, P. Krystek, **Absolute calibration of GNSS timing stations and its applicability to real signals**, Metrologia, 2018, 56(1), 015010.

[16] P. Waller, R. Valceschini, J. Delporte, **Cross-calibrations of multi-GNSS receiver chains**, 2019 Joint Conference of the IEEE International Frequency Control Symposium and European Frequency and Time Forum, IEEE, 2019, 1-4.

[17] K. Liang, T. Feldmann, A. Bauch, D. Piester, A. Zhang, **Performance evaluation of NIM GPS receivers in use for time transfer with PTB**, Proceedings of the 24th European Frequency and Time Forum (IEEE), 2010, pp. 1–8.

[18] Chinese National Metrology Technical Specification, **JJF 1403-2013: Calibration Specification for GNSS Receivers Used in Time Measurement** [In Chinese], 2013.

[19] K. Liang, T. Yu, Y. Li, X. Jiao, Y. Liu, J. Wang, **Absolute Calibration For Beidou Time Transfer Receiver**. XXIV IMEKO World Congress, 2024.